ELSEVIER

Atmospheric Research 59–60 (2001) 15–39

ATMOSPHERIC RESEARCH

www.elsevier.com/locate/atmos

The influence of deep convective motions on the variability of Z–R relations

Nikolai Dotzek *, Klaus D. Beheng

Institut für Meteorologie und Klimaforschung, Forschungszentrum/Universität Karlsruhe, Postfach 3640, D-76021 Karlsruhe, Germany

Received 15 January 2001; received in revised form 25 June 2001; accepted 23 July 2001

Abstract

Effects of deep convection on the precipitation rate R leading to variations in radar meteorological Z–R relations are studied. The basic contributions to this subject come from vertical and horizontal air motions as well as decreasing air density with height. Their influence on Z–R relations is investigated both with an analytical approach from cloud microphysics distinguishing between two characteristic spectral forms, and a mesoscale bulk model case study of a single cumulonimbus cloud. The precipitation rate is strongly affected by deep convective motions leading to increased mean value and standard deviation of the prefactor a in Z–R relations $Z=aR^b$. To a lesser extent, density stratification tends to diminish the prefactor. The exponent b, which can, without deep convection, vary from $b=1$ to $b=7/4$ depending on characteristic spectral form, remains unaffected by any of the dynamical effects studied here. Values of b can only be altered by such changes of the particle spectra, which affect the distribution of terminal velocity with hydrometeor size: in practice, this implies phase changes or variations in composition of the mixed-type hydrometeor ensemble. In spite of the variations in Z–R relations found in the present study, when performing an average over *the whole cloud and precipitation volume*, standard Z–R relations proposed for stagnant air still hold in a statistical sense. Furthermore, the effects of vertical air density gradients can be compensated, which should also help to improve quantitative rainfall estimates at large ranges from the radar site.

Keywords: Cloud microphysics; Convection; Z–R relation

* Corresponding author. Present affiliation: DLR-Institut für Physik der Atmosphäre, Oberpfaffenhofen, D-82234 Wessling, Germany. Tel.: +49-8153-28-1845; fax: +49-8153-28-1841.

E-mail address: nikolai.dotzek@dlr.de (N. Dotzek).

0169-8095/01/$ - see front matter
PII: S0169-8095(01)00107-7

1. Introduction

In hydrological applications, radar data are mostly evaluated to derive rain rates R at the ground from radar reflectivity η aloft. By definition, η resembles the scattering properties of an ensemble of hydrometeors. In the Rayleigh limit η is proportional to the sixth moment of the particle number density distribution $n(D)$, where D denotes particle diameter (e.g. Doviak and Zrnić, 1993). It can be computed as:

$$\eta = \frac{\pi^5}{\lambda^4}|K|^2 Z, \quad \text{with} \quad Z = \int_0^\infty n(D) D^6 \mathrm{d}D.$$

Thus, for constant wavelength λ, variations in η can result from (i) different hydrometeor types (i.e. phase changes) affecting the dielectric factor $|K|^2$ and (ii) variations in the number density distribution $n(D)$ affecting the radar reflectivity factor Z, or both. In general, η may change in time and space with an effectivity depending on several dynamical and especially microphysical factors.

The precipitation rate R, defined as vertical mass flux density of hydrometeors with bulk density ρ_h, i.e.

$$R = \frac{\pi}{6}\rho_h \int_0^\infty n(D) D^3 w_s \mathrm{d}D,$$

is, as Z, subject to certain variations in $n(D)$, but moreover depends on an effective sedimentation velocity w_s that is in detail:

$$w_\mathrm{s}(D, w, \rho) = w + w_\mathrm{t}(D, \rho) = w + f(\rho) w_{\mathrm{t},00}(D). \tag{1}$$

Here, w denotes ambient air vertical velocity, $w_{\mathrm{t},00}(D)$ is terminal velocity of hydrometeors at sea level conditions, and dependence of air density is given by $f(\rho)$. Variations of R, therefore, may result from up- and downdrafts as well as from vertical density gradients (Foote and du Toit, 1969; Kessler, 1969). Evidently, the rain rate for a given value of Z changes in space and time, and no unique Z–R relation exists in general. Also, if R at the ground (where $w = 0$) is derived from Z measured by low-elevation radar scans, the problem arises how to relate Z in a few kilometers above radar to an instantaneous rain rate at (or below) the radar level. Even in this case, vertical drafts and the profile of the horizontal wind may introduce considerable error to this nonlocal approach.

Although this issue had been raised previously (e.g. Battan, 1976; Zawadzki, 1984; Austin, 1987; Atlas et al., 1995; Yuter and Houze, 1997), to the authors' knowledge, it has never been quantified by computing the Z–R relation from the spectra $n(D)$. Our paper aims to give an example of such quantification by means of analytical calculations and a cloud-scale numerical case study of a convective shower cloud. Therein, we will address Z–R relationships locally within the cloud and its precipitation shaft. By giving up the nonlocal approach to relate R at the ground to Z somewhere aloft, we are in the position to study both the effects of deep convection and vertical density gradients on R and, hence, on Z–R. It will be clarified

- if in conditions of strong convection, other Z–R relations than the commonly accepted formulas should be applied;

- to what extent the spatio-temporal variations in Z–R relations reported in the literature can be attributed to the influence of deep convective motions.

The problem is tackled analytically in Section 2: after specification of hydrometeor spectra by Γ-type distribution functions for each class of particles, their radar reflectivity factor Z is derived as a function of hydrometeor content ρq per unit volume. Herein, q is the specific hydrometeor content (later on we will use index r for rain, c for cloud water, and i for cloud ice). Then, similar expressions for the precipitation rate R are given. The Z–R relations following from an elimination of ρq are then subjected to variations of R caused by changing air density and vertical motions. The choice of ρq as a main variable is motivated by the fact that following Kessler (1969), in most cloud-scale models, ρq is the only quantity to account for the presence of hydrometeors. In Section 3, such a model study is presented. High-resolution three-dimensional mesoscale model results for the case of a single cumulonimbus cloud are evaluated and compared to the analytical findings. Sections 4 and 5 present discussion and conclusions.

2. Analytical approach

Any analytical description of Z–R relationships relies on the choice of a mathematical representation of hydrometeor spectra. For unimodal mean spectra, many functional forms exists, of which the log-normal (e.g. Markowitz, 1976) and the Γ-function (e.g. Clark, 1974; Ulbrich, 1983, 1994) have been used most frequently. As the purely exponential size distribution proposed by Marshall and Palmer (1948) for raindrops is a special case of the Γ-function, we will also apply Γ-functions for our investigation. Recently, the need for universal, normalized forms of particle spectra has been expressed independently by several work groups (e.g. Sekhon and Srivastava, 1970, 1971; Willis, 1984; Sempere Torres et al., 1994, 1998; Haddad et al., 1996; Dotzek, 1999; Dou et al., 1999; Illingworth and Blackman, 1999) and, consequently, in our present study, the following normalized Γ-type distribution function is assumed for any hydrometeor type:

$$n(D) = N_0 \frac{\Gamma(4)}{\Gamma(\gamma+3)} \left(\frac{D}{D_0}\right)^{\gamma-1} \mathrm{e}^{-D/D_0}. \tag{2}$$

Here, D denotes particle diameter and γ is a shape parameter. N_0 is an amplitude or "particle load" of the distribution and D_0 is a formal scaling diameter (in fact, $D_0 \equiv 1/\lambda$ in the notation of Marshall and Palmer, 1948), which can easily be related to any specific measure of particle diameter, such as the volume median D_V as given in Appendix A. However, computations are facilitated greatly if D_0 is retained up to the final form of derived relations.

The use of a nondimensional spectrum according to Eq. (2) has some advantages compared to dimensional functions. First, the normalization in Eq. (2) assures that hydrometeor content ρq does not depend on the shape parameter γ (cf. Eq. (4)) and that for $\gamma = 1$, the exponential Marshall and Palmer (1948) spectrum is reproduced. Second,

Table 1
Number and volume median diameters for various values of the shape parameter γ
For definition of D_N and D_V, see Eq. (36). The nondimensional location of the spectral peak ($D_{\max}$, $n_{\max}$) is also given.

γ	$n_{\max}/N_0$	$D_{\max}/D_0$	D_N/D_0	D_V/D_0
1.0	1.0×10^{0}	0.0	0.693	3.672
2.0	9.2×10^{-2}	1.0	1.678	4.671
3.0	2.7×10^{-2}	2.0	2.674	5.670
4.0	1.1×10^{-2}	3.0	3.672	6.670
5.0	5.6×10^{-3}	4.0	4.671	7.669
6.0	3.1×10^{-3}	5.0	5.670	8.669
7.0	1.9×10^{-3}	6.0	6.670	9.669
8.0	1.2×10^{-3}	7.0	7.669	10.668
9.0	8.5×10^{-4}	8.0	8.669	11.668
10.0	6.0×10^{-4}	9.0	9.669	12.668

both $n(D)$ and N_0 are given in units of m^{-4}, or conventionally in $\mathrm{mm}^{-1}\,\mathrm{m}^{-3}$. The shape of the spectrum is characterized by a maximum at

$$D_{\max} = D_0(\gamma - 1), \quad n_{\max} = n(D_{\max}) = N_0 \frac{\Gamma(4)}{\Gamma(\gamma + 3)} (\gamma - 1)^{\gamma - 1} \mathrm{e}^{-(\gamma - 1)}.$$

Normalized values for $D_{\max}$ and $n_{\max}$ are given in Table 1. With increasing γ, the spectra broaden and conserve ρq by lowering $n_{\max}$. For later use, we define the moment M_m of order m by

$$M_m = \int_0^\infty n(D) D^m \mathrm{d}D = \frac{\Gamma(4)}{\Gamma(\gamma + 3)} \Gamma(\gamma + m) N_0 D_0^{m+1}. \tag{3}$$

As most bulk microphysics cloud models following the work of Kessler (1969) use hydrometeor content ρq as the main prognostic variable, this quantity will also be applied in this paper:

$$\rho q = \frac{\pi}{6} \rho_h \, M_3 = \pi \rho_h N_0 D_0^4. \tag{4}$$

Spectral parameters can be substituted by the moments M, so the quantity ρq from Eq. (4) will be introduced to any following equation to eliminate either N_0 or D_0, depending on which spectral parameter aside from ρq is chosen to describe the particle spectrum. Note that this does not imply any loss of generality for the spectra. Neither N_0, D_0, γ nor ρq are assumed as constant, and all these quantities can be functions of time and space.

2.1. Radar reflectivity factor

The radar reflectivity factor Z for spherical particles under the assumption of Rayleigh's approximation (radar wavelength much larger than particle size) is given by

$$Z = M_6 = \Gamma(4) \frac{\Gamma(\gamma + 6)}{\Gamma(\gamma + 3)} N_0 D_0^7 = \Gamma(4)(\gamma + 5)(\gamma + 4)(\gamma + 3) N_0 D_0^7, \tag{5}$$

and has unit m^3, or conventionally $mm^6\ m^{-3}$. Now, from Eq. (4), we arrive at the following two desired relationships between Z and ρq by eliminating either D_0 or N_0:

$$Z = \frac{\Gamma(4)}{[\pi\rho_h]^{7/4}}(\gamma+5)(\gamma+4)(\gamma+3)N_0^{-3/4}(\rho q)^{7/4}, \tag{6a}$$

$$Z = \frac{\Gamma(4)}{\pi\rho_h}(\gamma+5)(\gamma+4)(\gamma+3)D_0^3\ \rho q. \tag{6b}$$

Note that the Z–R relation of Eq. (6b) being linear in ρq is related to hydrometeor spectra, which have been reported to occur only rarely (Waldvogel, 1974). In effect, most published Z–ρq relations show the power 7/4 (Kessler, 1969) or similar empirical values like 1.63 (Hauser et al., 1988), 1.82 (Douglas, 1964; Smith et al., 1975) for rain or 1.67 (Liu and Illingworth, 2000), 1.79 (Bielli and Roux, 1999) for cloud ice. Clearly, Z does not depend on either vertical velocity or on the variation of fall speed due to the vertical density gradient.

2.2. Mean terminal fall velocity

Specifying the index "00" for all quantities at the chosen reference level, i.e. sea level conditions with vertical air velocity $w=0$, air density $\rho=\rho_{00}=1.225\ kg\ m^{-3}$, first the terminal fall velocity $w_{t,00}$ of the hydrometeors as a function of ρq in this basic case will be computed by setting

$$w_{t,00}(D) = w_0\left(\frac{D}{\hat{D}}\right)^{\beta}. \tag{7}$$

Here $\hat{D}$ is the unit diameter, usually 1 mm and w_0 is the terminal fall velocity of hydrometeors with $D\equiv\hat{D}$. For rain, Kessler (1969) proposed $w_0=-4.11\ m\ s^{-1}$ and $\beta=1/2$. Using Eq. (7), a volume-weighted mean fall velocity $\overline{w}_{t,00}$ can be calculated:

$$\overline{w}_{t,00} = \frac{\pi\rho_h}{6\rho q}\int_0^\infty n(D)w_{t,00}(D)D^3\,\mathrm{d}D, \tag{8}$$

which is, after multiplication by ρq, identical to the mean mass flux density or precipitation rate R. In Eq. (8), again either N_0 or D_0 can be eliminated introducing the hydrometeor content from Eq. (4):

$$\overline{w}_{t,00} = \frac{w_0}{[\pi\rho_h]^{\beta/4}}\frac{\Gamma(\gamma+3+\beta)}{\Gamma(\gamma+3)}D^{-\beta}N_0^{-\beta/4}(\rho q)^{\beta/4}, \tag{9a}$$

$$\overline{w}_{t,00} = w_0\frac{\Gamma(\gamma+3+\beta)}{\Gamma(\gamma+3)}\left(\frac{D_0}{\hat{D}}\right)^{\beta}. \tag{9b}$$

Note that Eq. (9b) is independent of ρq. Rain rates and Z–R relations will subsequently be given considering both Eqs. (9a) and (9b).

2.3. Z–R relation at sea level

Following Eq. (1), in its most general form, the sedimentation velocity of a single hydrometeor reads

$$w_s(D, w, \rho) = w + w_{t,00}(D)\left(\frac{\rho_{00}}{\rho}\right)^{\alpha},$$

which in terms of mean values after integration over the entire particle spectrum as in Eq. (8) yields:

$$\overline{w}_s(w, \rho) = w + \overline{w}_{t,00}\left(\frac{\rho_{00}}{\rho}\right)^{\alpha}. \tag{10}$$

Here w denotes any ambient vertical air velocity, reference level terminal velocity $\overline{w}_{t,00}$, and a height dependence $f(\rho)$ with exponent α ranging from 0.4 (Foote and du Toit, 1969) to 0.5 (Kessler, 1969). It is obvious that w_s is an effective fall velocity subsuming contributions by vertical air motions and the density dependence of the air drag exerted on hydrometeors.

The generic precipitation rate R or the vertical hydrometeor mass flux density in kg m^{-2} s^{-1} is then given by

$$R = \frac{\pi}{6}\rho_h \int_0^{\infty} n(D) w_s(D, w, \rho) D^3 \mathrm{d}D = -\overline{w}_s(w, \rho)\rho q, \tag{11}$$

which by virtue of the mean value theorem can be expressed by the right hand side of Eq. (11), linking both mean sedimentation velocity $\overline{w}_s$ and hydrometeor content. Conventionally, R is taken to be a positive definite quantity even though precipitation *falling* to the ground requires a negative $\overline{w}_s$ and hence implies a negative definite R. This is the reason for the minus sign in Eq. (11).

To derive first R and subsequently the Z–R relation under the above-mentioned reference conditions at sea level, we see from $\overline{w}_s = \overline{w}_{t,00}$ that in this basic case, R reduces to

$$R = -\overline{w}_{t,00}\rho q. \tag{12}$$

Using Eqs. (9a) and (9b), this leads to

$$R = \frac{-w_0}{(\pi\rho_h)^{\beta/4}} \frac{\Gamma(\gamma + 3 + \beta)}{\Gamma(\gamma + 3)} \hat{D}^{-\beta} N_0^{-\beta/4} (\rho q)^{1+\beta/4}, \tag{13a}$$

$$R = -w_0 \frac{\Gamma(\gamma + 3 + \beta)}{\Gamma(\gamma + 3)} \left(\frac{D_0}{\hat{D}}\right)^{\beta} \rho q. \tag{13b}$$

With Eqs. (6a), (13a) and (6b), (13b), respectively, and after some tedious calculations, the corresponding Z–R relations read

$$Z = a_{00,N} R^{7/(4+\beta)}, \quad \text{with} \quad a_{00,N} = \frac{\Gamma(4)}{(-\pi\rho_{\mathrm{h}} w_0)^{7/(4+\beta)}} (\gamma+5)(\gamma+4)(\gamma+3) \times \left[\frac{\Gamma(\gamma+3)}{\Gamma(\gamma+3+\beta)}\right]^{7/(4+\beta)} N_0^{-(3-\beta)/(4+\beta)} D^{7\beta/(4+\beta)}, \tag{14a}$$

$$Z = a_{00,D} R, \quad \text{with} \quad a_{00,D} = \frac{\Gamma(4)}{-\pi\rho_{\mathrm{h}} w_0} \frac{\Gamma(\gamma+6)}{\Gamma(\gamma+3+\beta)} D_0^{3-\beta} D^{\beta}. \tag{14b}$$

Applying Kessler's β-value for raindrops, i.e. $\beta = 1/2$, Eq. (14a) becomes $Z = a_{00,N} R^{14/9}$ with a power of $14/9 \simeq 1.56$. We see further that choice of the characteristic spectral form (elimination of either D_0 or N_0 by ρq) causes significant differences in exponent b. These, however, do not stem from deep convection.

2.4. Z–R relation in deep layers

After studying the special case $\overline{w}_{\mathrm{s}} = \overline{w}_{\mathrm{t},00}$ (implying $w = 0$ and $\rho = \rho_{00}$), we will first examine density effects on the Z–R relation and then also allow for $w \neq 0$ as in convective clouds.

2.4.1. Stagnant air

Using Eq. (11) again and setting only $w = 0$ in Eq. (10), the precipitation rate now becomes

$$R = -w_{\mathrm{t},00} \left(\frac{\rho_{00}}{\rho}\right)^{\alpha} \rho q, \tag{15}$$

so that Eqs. (14a) and (14b) yield, respectively,

$$Z = a_{00,N} f_N(\rho) R^{7/(4+\beta)}, \quad \text{with} \quad f_N(\rho) = \left(\frac{\rho_{00}}{\rho}\right)^{-\alpha[7/(4+\beta)]}, \tag{16a}$$

$$Z = a_{00,D} f_D(\rho) R, \quad \text{with} \quad f_D(\rho) = \left(\frac{\rho_{00}}{\rho}\right)^{-\alpha}. \tag{16b}$$

Note that the density variations only affect the prefactor of the two characteristic Z–R relations. The only variable entering their exponent is the value β from the terminal fall velocity power law.

It is clearly seen that Eqs. (14a), (14b), (16a) and (16b) all represent specific formulations of the commonly applied Z–R relation

$$Z = aR^b.$$

To get an impression of the variability in superscript b resulting from our calculations, Fig. 1 compiles various typical ranges of b. For hydrometeors falling at a constant terminal velocity $w_{\mathrm{t},00}(D) = \text{const}$, i.e. $\beta = 0$ in Eq. (7) as an upper limit $b = 7/4$ follows. Most slopes of observed Z–R relations fall in the range $7/5 \leq b \leq 7/4$, where the value

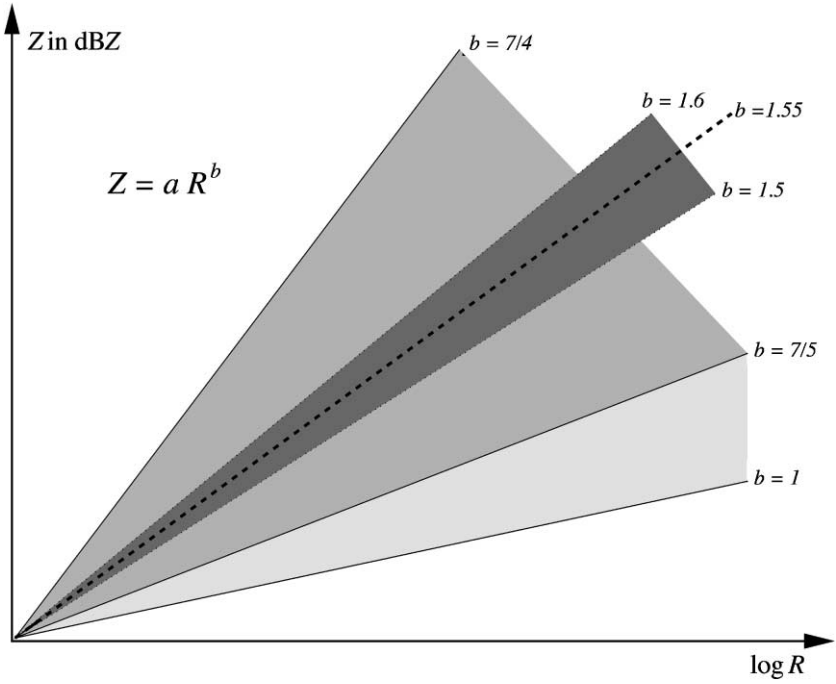

Fig. 1. Schematic representation of different ranges in slope b of Z–R relations derived from analytical considerations. For relations of the form $Z=aR^b$, the lower limit $b=1$ follows for a constant diameter D_0. The light shaded range $[1 \leq b < 7/5]$ is seldom observed but not in principle excluded by theory. The medium shaded range $[7/5 \leq b \leq 7/4]$, however, covers all cases depending on N_0 and varying vertical velocities $w_{t,00}$. The most probable range for the exponent $b=1.55\pm0.05$ is given by the dashed line and the dark shaded area. An upper limit $b=7/4$ follows for $w_{t,00}=\text{const}$.

of 7/5 corresponds to linear laws $w_{t,00}(D)$. The slope $b\simeq1.55\pm0.05$ most often reported in the literature (e.g. Battan, 1973; Hauser et al., 1988; Sauvageot, 1992; Rinehart, 1997) corresponds to roughly $w_{t,00}(D)\propto D^{1/2}$, i.e. $\beta=1/2$ and raindrop-dominated precipitation (Kessler, 1969; Pruppacher and Klett, 1997). Values of b smaller than 7/5 are seldom reported as they would correspond to $\beta>1$ or other particular meteorological conditions, cf. Battan (1973, Table 7.1, pp. 90–91) and Aniol et al. (1980). The lower limit $b=1$ follows for equilibrium raindrop spectra (Zawadzki and de Agostinho Antonio, 1988) or spectra with a constant D_0, which have been identified to occur only rarely (Waldvogel, 1974). Note that the same ranges of b were found by Dölling et al. (1998) from an evaluation of disdrometer data.

2.4.2. Convection

Finally, we discuss the general case in which an external vertical velocity field w is imposed so that with Eq. (10) the precipitation rate then reads

$$R = -\overline{w}_s \rho q = -\left[w + \overline{w}_{t,00} \left(\frac{\rho_{00}}{\rho} \right)^{\alpha} \right] \rho q. \tag{17}$$

Without loss of generality, we set

$$w = X\ \overline{w}_{\mathrm{t},00}\left(\frac{\rho_{00}}{\rho}\right)^{\alpha}, \quad -1 < X < \infty. \tag{18}$$

Here negative values of X correspond to updrafts, and $X \leq -1$ is excluded as it corresponds to floating or even rising particles. Our X-factor approach covers the following two extreme cases:

1. an arbitrary value of w is imposed on the hydrometeor field, i.e. no coupling of w and ρq. In this case, X is the variable maintaining the given w in an inhomogeneous $\overline{w}_{\mathrm{t},00}$ field: $X \stackrel{\mathrm{def}}{=} w/\overline{w}_{\mathrm{t},00}(\rho_{00}/\rho)^{-\alpha}$.
2. w is strictly proportional to $\overline{w}_{\mathrm{t},00}$ in the hydrometeor field, i.e. complete coupling of w and ρq. In this case, w is the variable maintaining the given X in an inhomogeneous $\overline{w}_{\mathrm{t},00}$ field: $w \stackrel{\mathrm{def}}{=} X\ \overline{w}_{\mathrm{t},00}(\rho_{00}/\rho)^{\alpha}$.

Definitely, reality will be in between the two alternatives (and probably closer to the first). The local value of w is a superposition of an imposed vertical wind and an additional downdraft component induced by the hydrometeor drag. Introducing Eq. (18) into Eq. (17), the expression for the rain rate becomes

$$R = -(X+1)\overline{w}_{\mathrm{t},00}\left(\frac{\rho_{00}}{\rho}\right)^{\alpha}\rho q. \tag{19}$$

Inserting Eq. (19) in Eqs. (16a) and (16b), respectively, leads to

$$Z = a_{00,N} f_N(\rho) g_N(w) R^{7/(4+\beta)}, \quad \text{with} \quad g_N(w) = (X+1)^{-7/(4+\beta)}, \tag{20a}$$

$$Z = a_{00,D} f_D(\rho) g_D(w) R, \quad \text{with} \quad g_D(w) = (X+1)^{-1}. \tag{20b}$$

Note that any vertical air motions again only affect the prefactor of the two relations. This statement holds in a very general sense; we have not limited ourselves in this analytical investigation concerning the variability of spectral parameters (N_0, D_0, γ, ρq) in space and time. Obviously, the exponent b could be altered if the value of β, i.e. the fall speed power law, would change. Referring to Eq. (7), it is apparent that usually, transitions from one hydrometeor type to another have to take place (e.g. droplets to ice crystals) to introduce modified values of w_0 and β. If the hydrometeor type or mixture does not change, say in a warm cloud situation in which raindrops do not freeze and raindrops collect only cloud droplets or other raindrops, then $n(D)$ could be subject to arbitrary variations and yet the fall speed power law would remain unaffected. This holds because Eq. (7) is a general description for terminal velocity as a function of diameter for one specific hydrometeor class.

3. Modeling case study

The modeling results presented in this section will help to further quantify the analytical results from a different point of view. For the model experiment to investigate Z–R relations, the three-dimensional nonhydrostatic Karlsruhe Atmospheric Mesoscale Model (KAMM) (Adrian and Fiedler, 1991) was applied in a substantially revised and

extended version suitable to simulate deep convection including a bulk microphysical cloud module predicting rain water ρq_r, cloud water ρq_c, and cloud ice ρq_i (Dotzek, 1998, 1999). Aside from the prognostic quantity ρq, the model also provides the fields of w, ρ and terminal fall speed of hydrometeors $\bar{w}_{t,00}$. As for the analytical approach, all hydrometeor fall speeds in the model are subject to a variation due to density stratification according to Eq. (15) with $\rho_{00} = 1.225$ kg m^{-3} and $\alpha = 0.4$.

We have to mention here that the bulk microphysics description in the model is less general compared to our analytical approach in Section 2. In the KAMM model, particle spectra are held fixed (N_0, γ), and only ρq is variable. Nevertheless, we will be able to study the effects of vertical drafts and air density changes, and also (although simplified) the influence of mixtures of hydrometeors with different fall speed laws. As shown in Section 2, the former should modify prefactor a, the latter exponent b of Z–R relations $Z = aR^b$.

The model domain chosen was 64 km in both horizontal directions x and y. The top of the domain was at 18 km above sea level (ASL) and in the center of the domain, an idealized 500-m high bell-shaped mountain (indicated by dashed circles in Fig. 2) rose from the otherwise flat grass-covered terrain. Spatial resolution of the model was 1 km horizontally and 10 m (at the ground) to about 100 m (near the model top) vertically. The basic state of this model run was a barotropic flow of 10 m s^{-1} from west-southwest, and the profiles of temperature and humidity allowed for cloud tops at 8–9 km ASL.

Convection was initiated by a local boundary layer perturbation to the basic state, a moist and warm air bubble at ($x = 10$, $y = 25$), similar to the procedure of Klemp and Wilhelmson (1978). The bubble was introduced to the system after 1 h of simulation, i.e. at 1200 local standard time (LST). Fig. 2 shows a synthetical radar composite from the model study. It is a Maximum Constant Altitude Plan Position Indicator (MAX_CAPPI) of the radar reflectivity factor, showing the projection of the highest Z-values in the volume data to the Cartesian planes x,y (large panel), x,z (small upper panel), and y,z (small right panel). Light grey shading outlines the cloud shape, dark grey areas correspond to high reflectivities of more than 40 dBZ.

Soon after initiation, a rapidly developing cumulus cloud appeared, moving east–northeastward with the mean flow. As Fig. 2 reveals, at 1220 LST, cloud top was at about 7 km ASL (a) and a core of high reflectivity has developed. Only 10 min later, strong precipitation fell out of the now mature cumulonimbus cloud with its top at 9 km ASL (b). The decaying stage with weakening precipitation and cloud transition to an ice-filled anvil can be seen from image (c) from 1245 LST. The highest computed reflectivities in this storm were above 60 dBZ, the initial instantaneous rain rate at the ground peaked at 420 mm h^{-1}, and the largest precipitation accumulation at a single point was 34 mm. Updrafts in this cloud hardly exceeded 11 m s^{-1} (at 1220 LST), downdrafts reached their peak of about -10 m s^{-1} at 1245 LST, and only a weak gust front developed at later times. To sum up, this small cumulonimbus cell is by no means exceptional. Instead, it represents the typical Central European heavy rain shower during summer and was therefore chosen as a representative case to study the effects of convection on the Z–R relation. For completeness, we mention that the shallow boundary layer cloud (d) at the right side of the model domain in Fig. 2 is a stationary, orogenic

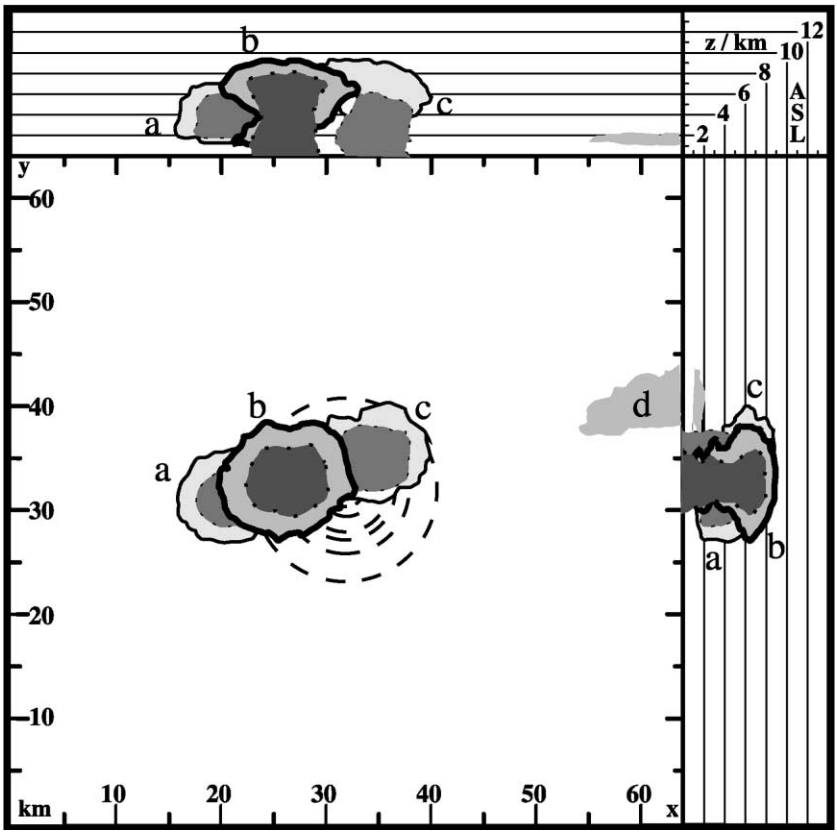

Fig. 2. Synthetical radar composite of the modeled storm: projection of maximum reflectivities onto Cartesian planes, MAX_CAPPI-*Z*. Letters denote three different stages of cumulonimbus development, (a) 1220 LST growth, (b) 1230 LST maturity, and (c) 1245 LST decay. Light grey shading shows the cloud dimensions, regions with $Z \geq 40$ dB*Z* appear in dark grey. Stage (b) being the basis of our case study has been highlighted for clarity. A stationary shallow boundary layer cloud (d) has formed in the lee of the 500-m bell-shaped mountain (dashed circular height contours) in the center of the model domain.

stratocumulus which had formed from near-surface horizontal convergence in the lee of the bell-shaped mountain.

The radar reflectivity factors shown in Fig. 2 represent the total sum of *Z*-values from any present hydrometeors. For comparison with our analytical findings, however, their separate contributions to total reflectivity will be considered. Therefore, even though Figs. 3–5 show *Z*–*R* relations for cloud ice and cloud water as well, the quantitative evaluation is focused on the model-predicted precipitation ρq_r which can, depending on ambient temperature, behave like either rain, snow/lump graupel, or a mixture of both.

For raindrops, the KAMM model uses the terminal velocity formulation first applied by Soong and Ogura (1973) and later on by Klemp and Wilhelmson (1978):

$$\overline{w}_{t,00} = -14.16 \text{ m s}^{-1} \left(\frac{\rho q_r}{\text{kg m}^{-3}} \right)^{0.1364} . \quad (21)$$

Comparing this relation to Eq. (9a), two things should be noted: the value $-14.16\ \mathrm{m\ s^{-1}}$ corresponds to the complete set of factors preceding $(\rho q)^{\beta/4}$ (not only to w_0), and the exponent implies $\beta = 4 \times 0.1364 = 0.5456$, fairly central in the accepted range $[0 \leq \beta \lesssim 1]$ for $w_{\mathrm{t},00}(D)$ power laws (cf. Fig. 1). The analytical Z–R relation for rain from Eqs. (6a) and (21) and the R–ρq relation from Eq. (15) in SI units read

$$Z = \frac{\Gamma(4)}{(\pi\rho_{\mathrm{h}})^{7/4}} 14.16^{-7/(4+\beta)} (\gamma+5)(\gamma+4)(\gamma+3) N_0^{-3/4} \left(\frac{\rho_{00}}{\rho}\right)^{-\alpha[7/(4+\beta)]} \times R^{7/(4+\beta)}, \tag{22}$$

$$R = 14.16 \left(\frac{\rho_{00}}{\rho}\right)^{\alpha} \left(\frac{\rho q_{\mathrm{r}}}{\mathrm{kg\ m^{-3}}}\right)^{1.1364}. \tag{23}$$

For a pure exponential spectrum ($\gamma = 1$) with $N_0 = 8.0 \times 10^6\ \mathrm{m^{-4}}$ as standard value (Marshall and Palmer, 1948), the same relations in conventional units become

$$\frac{Z}{\mathrm{mm^6\ m^{-3}}} = 205 \left(\frac{\rho_{00}}{\rho}\right)^{-1.54\alpha} \left(\frac{R}{\mathrm{mm\ h^{-1}}}\right)^{1.54},$$

$$\frac{R}{\mathrm{mm\ h^{-1}}} = 19.90 \left(\frac{\rho_{00}}{\rho}\right)^{\alpha} \left(\frac{\rho q}{\mathrm{g\ m^{-3}}}\right)^{1.1364}. \tag{24}$$

The exponent $b = 7/(4+\beta) \simeq 1.54$ agrees very well with our analytical findings and the experimental data of Dölling et al. (1998). Again, only the prefactor of this relation depends on air density. Note that using $Z = 2.4 \times 10^4\ (\rho q)^{1.82}$ (Douglas, 1964; Battan, 1973; Smith et al., 1975) yields $Z = 199R^{1.6}$. Kessler (1969) reported $Z = 210R^{14/9}$ and $R = 18.35(\rho q)^{9/8}$ for sea level conditions, so on average $200R^{1.6}$ is supported (Marshall and Palmer, 1948; Battan, 1973).

Effects of mixed and ice-phase precipitation were included in the KAMM model according to the simple approach by Tartaglione et al. (1996): below freezing level height, Eq. (21) proposed by Soong and Ogura (1973) is applied. Above the freezing level, hydrometeor fall speeds are computed as temperature-weighted averages between raindrop fall speed (Eq. (21)) and a constant terminal velocity (implying $\beta = 0$)

$$\overline{w}_{\mathrm{t},00} = -2.5\ \mathrm{m\ s^{-1}}, \tag{25}$$

representative of a mixture of snow and lump graupel (Locatelli and Hobbs, 1974; Starr and Cox, 1985). For temperatures less than $-35\ ^{\circ}\mathrm{C}$, only this asymptotic fixed value is assumed. As Tartaglione et al. (1996) were able to show, storm dynamics are improved significantly by this more realistic description of hydrometeor sedimentation.

Evaluation of the asymptotic case of constant fall speed from Eq. (25) yields Z–R and R–ρq relations using Eqs. (15) and (16a)

$$Z = \frac{\Gamma(4)}{(\pi\rho_{\mathrm{h}} 2.50)^{7/4}} (\gamma+5)(\gamma+4)(\gamma+3) N_0^{-3/4} \left(\frac{\rho_{00}}{\rho}\right)^{-\alpha 7/4} R^{7/4}, \tag{26}$$

$$R = 2.50 \left(\frac{\rho_{00}}{\rho}\right)^{\alpha} \frac{\rho q_{\mathrm{r}}}{\mathrm{kg\ m^{-3}}}, \tag{27}$$

or in conventional units and under the same assumptions, as in Eq. (24):

$$\frac{Z_e}{\mathrm{mm^6\ m^{-3}}} = 73\left(\frac{\rho_{00}}{\rho}\right)^{-\alpha 7/4}\left(\frac{R}{\mathrm{mm\ h^{-1}}}\right)^{7/4}, \quad \frac{R}{\mathrm{mm\ h^{-1}}} = 9.02\left(\frac{\rho_{00}}{\rho}\right)^{\alpha}\frac{\rho q}{\mathrm{g\ m^{-3}}}. \tag{28}$$

The equivalent reflectivity factor Z_e of ice particles was computed under the assumption of a melted drop spectrum according to Smith (1984): $Z_e = 0.225Z$.

We now turn to incorporate results obtained with the KAMM model for the storm shown in Fig. 2. The three characteristic stages of cloud development depicted in this MAX_CAPPI–Z composite could either be chosen as a basis for our investigation without altering the outcome much. Decision was made to focus on stage (b), cloud maturity, for the reason that here maximum up- and downdrafts were nearly in equilibrium ($w_{max} = 5.8$ m s^{-1}, $w_{min} = -5.1$ m s^{-1}). Therefore, there should be negligible bias due to any preference to the sign of vertical motions. Results from stages (a) and (c) in Fig. 2 have been checked to yield similar statistics, although in stage (a), storm growth, a greater volume of cloud and precipitation experiences updrafts ($w_{max} = 11.1$ m s^{-1}, $w_{min} = -2.0$ m s^{-1}) and reduced rain rates, while in stage (c), storm decay, rain rates tend to be enhanced due to more dominant downdrafts ($w_{max} = 3.2$ m s^{-1}, $w_{min} = -9.8$ m s^{-1}).

3.1. Stagnant air

Neglecting first the Tartaglione et al. (1996) mixed-phase fall speed parameterization and treating all precipitation ρq_r as rain drops, we obtain the scatter plot of Z–R relations shown in Fig. 3 for the modeled cumulonimbus cloud of Fig. 2, stage (b). For all grid points within the cloud and the rain shaft, both Z and R were evaluated from the hydrometeor concentrations ρq and depicted as symbols in the diagram. The letters r, i, and c denote the Z–R relations for precipitation (+), cloud ice (*), and cloud water (○), respectively. While the latter two are mainly given for completeness and to demonstrate the model's ability to "measure" extremely small sedimentation rates, the analysis of the data focuses on the relation for rain. Therefore, the index r will be omitted for simplicity from the relations given below.

Obviously, for this case in which only density variations from the factor $f_N(\rho)$ are present, the model data reproduce Eq. (24) very well, although the density dependence introduces a ±1.5 dBZ scatter for any value of rain rate. A regression analysis for $R \geq 10^{-6}$ mm h^{-1} yields

$$Z = [173 \pm 24]R^{1.55\pm0.01}, \quad R = [22.08 \pm 1.94](\rho q)^{1.13\pm0.01}, \tag{29}$$

and shows that, indeed, only the prefactor is affected by effects of density stratification. The small standard deviation in the exponent must be attributed to be a purely statistical artifact of the regression algorithm—as the analytical reasoning showed, the power b remains unaffected by all the physical mechanisms studied here.

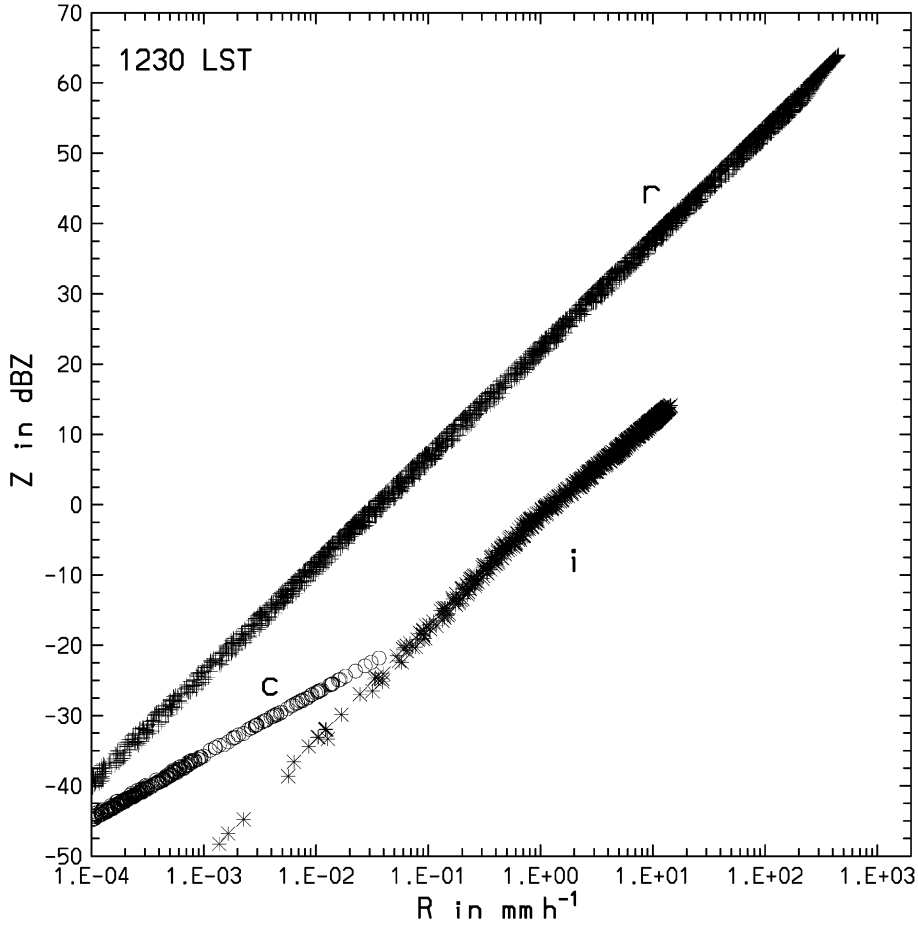

Fig. 3. Z–R relations in the KAMM model study for stagnant air, only including the effect of density variations after Foote and du Toit (1969). Letters at the curves indicate rain (r,+), cloud water (c, ○), and cloud ice (i, *).

Evaluating the same case but applying now the temperature-dependent fall speed parameterization by Tartaglione et al. (1996) for mixed and ice-phase precipitation, Fig. 4 depicts the consequences for one and the same data as in Fig. 3. While curves (c) and (i) for cloud particles remain unaffected, the Z–R relation for precipitation particles is now split in two—branch (r) corresponds to Eq. (29) and branch (s) with its steeper slope outlines the limiting case of constant fall speed for the ice-phase. Fewer points between branches (r) and (s) indicate mixed-phase precipitation (wet snow/graupel). Both curves yield similar values for high precipitation rates but start to separate for $R < 10$ mm h^{-1}. The relationship in the asymptotic case (s) with dry snow or graupel only is

$$Z_e \simeq 56R^{1.75}, \quad R \simeq 12.88\rho q^{1.00}, \tag{30}$$

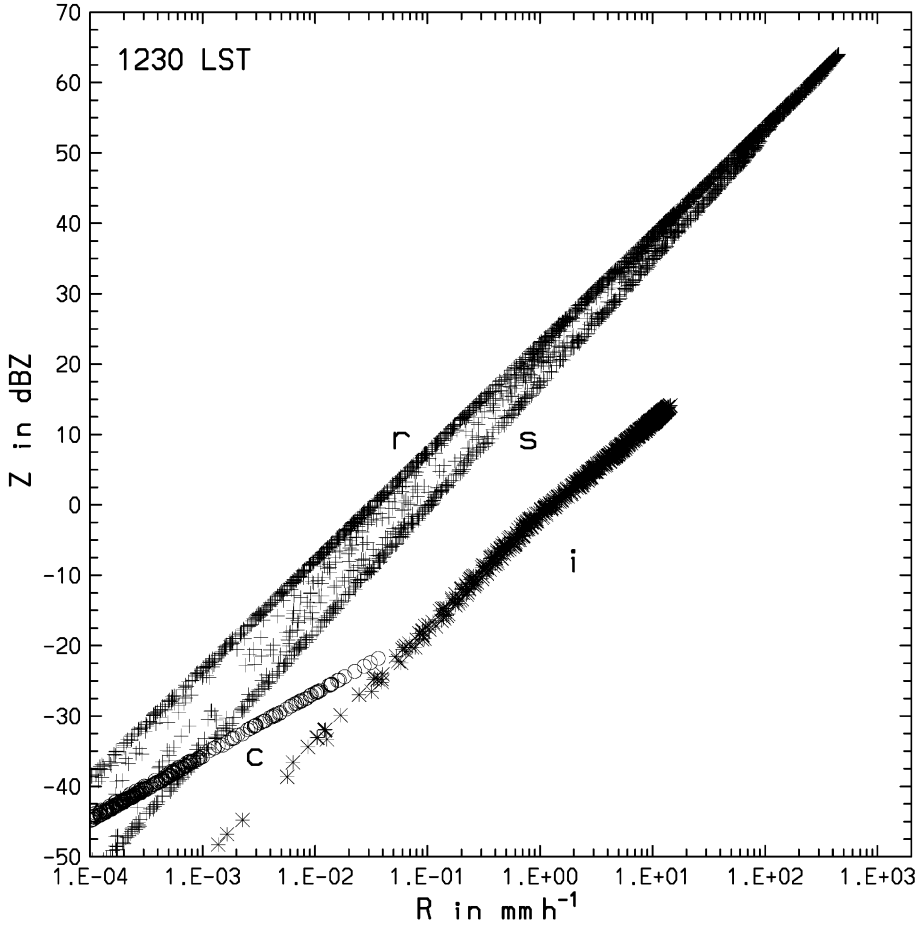

Fig. 4. As Fig. 3, yet including the simple mixed-phase precipitation fall speed parameterization of Tartaglione et al. (1996). This adds an asymptotic branch (s) to the rain $Z-R$ relation, corresponding to the case of snow/lump graupel with $\overline{w}_{t,00}=\text{const}$ assumed.

with the exponent $b=7/4$ as expected. Again, the higher precipitation rate aloft reduces the prefactor in the modeled $Z-R$ relation without changing b, as can be seen by comparison to Eq. (28).

3.2. Deep convection

Both Eqs. (29) and (30) excluded vertical air motions in the analysis. As the mesoscale model provides the field w at any grid point, these convective motions can easily be added when computing the local precipitation rate. Up- and downdraft speeds in the cumulonimbus cloud at the stage (b) in Fig. 2 were still in excess of 5 m s^{-1}, so some portions of the hydrometeors were no longer descending to the ground but rising upward. As these would lead to negative values of precipitation rate R, they were not

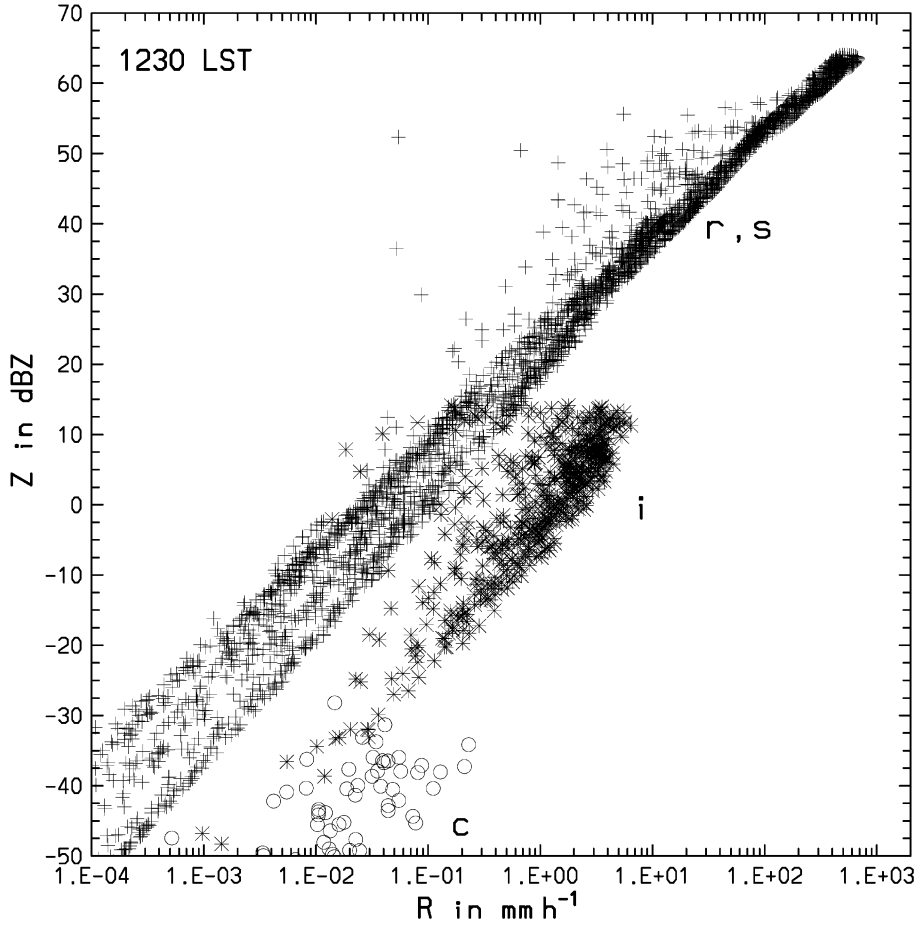

Fig. 5. As Fig. 4, but also including any modeled convective vertical motions within the cumulonimbus cell and its precipitation at the point of mature cloud development, (b) in Fig. 2.

considered in the following evaluation. Naturally, slowly subsiding hydrometeors like cloud ice and especially cloud droplets are most affected by updrafts and their Z–R relations will suffer the largest loss of data points.

This can be seen in Fig. 5. As in Figs. 3 and 4, this scatter plot shows Z–R points from the total cloud and precipitation volume. Therefore, the data are not specific for a certain height level but for the whole rainstorm. Apparently, the Z–R relations for cloud water and cloud ice are hardly discernible any more. Only for precipitation rates of more than 0.1 mm h^{-1}, the cloud ice data group into a denser cluster with a roughly linear trend. For the mixed-phase precipitation, however, and $R \geq 0.05$ mm h^{-1}, the data from the two asymptotic cases of rain and snow/lump graupel now collapse on a linear curve on average:

$$Z = [202 \pm 95]R^{1.54\pm0.11}, \quad R = [18.46 \pm 7.23](\rho q)^{1.13\pm0.10}. \tag{31}$$

The error bars give the standard deviation determined from linear regression analysis. Therefore, even for rapidly falling precipitation hydrometeors, the data are very noisy and have numerous outliers relative to the mean relation with combinations of high reflectivity factors and very small precipitation rates. These result from large hydrometeor contents within the main updraft core. For some of these data points, $\overline{w}_s$ has become so small that the rain rate is reduced by a factor of 100 compared to the rain rate in stagnant air. On the contrary, in the main downdraft within the rain shaft, R is increased by a factor of 2.

Comparison with Eq. (20a) shows that these variations imply a range of X $[-0.99 \lesssim X \lesssim 2.00]$.

For more intense convective clouds with higher downdraft intensities, this range would be expanded, especially for positive X. But even the moderate variation in X suffices to introduce an uncertainty of $\pm 47\%$ in the prefactor of the average Z–R relation as shown in

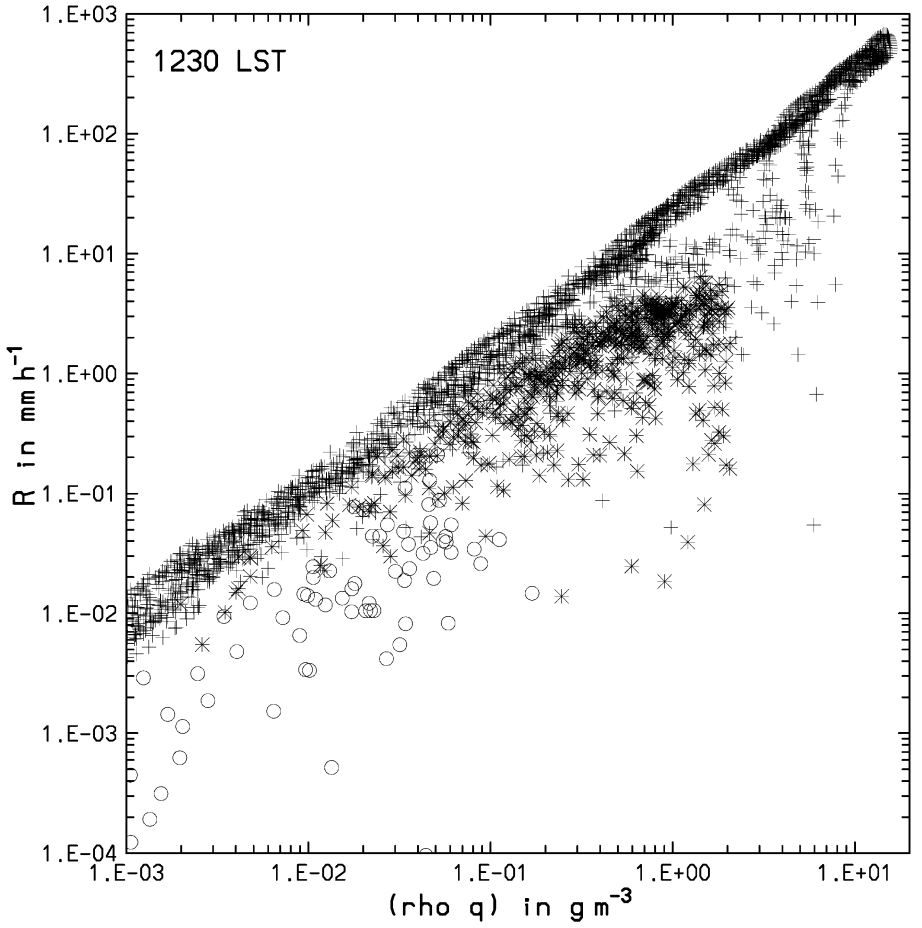

Fig. 6. R–ρq relations under the same conditions as in Fig. 5 for mixed-phase precipitation (+), cloud water (○), and cloud ice (*).

Eq. (31). This noise cannot be attributed to any different asymptotic relations for rain and snow: Fig. 4 shows that the spread between branches (r) and (s) is small for relevant rain rates, i.e. $R \gtrsim 0.1$ mm h^{-1}. Instead, vertical air motion causes the large observed scatter in Z and R.

Also note from comparing Eqs. (29) and (31) that, as anticipated in Section 2, introduction of a *mixture* of hydrometeors with *different* fall speed laws causes an effect on the Z–R law exponent b. In this simplified bulk model study, mean value and standard deviation change due to the presence of only two different hydrometeor types from $b = 1.55 \pm 0.01$ to a power of $b = 1.54 \pm 0.11$.

Any effects of vertical drafts on R alone are further substantiated by Fig. 6 showing a scatter plot of ρq, R for precipitation (+), cloud water (○), and cloud ice (*) from the same volume data as in Fig. 5. Obviously, the highest reductions of R occur for large hydrometeor contents ($\gtrsim 2$ g m^{-3} for rain, $\gtrsim 1$ g m^{-3} for cloud ice). Individual grid points in the precipitation volume show an updraft-induced reduction in R to less than 1%, similar values are found for ice. Even more obvious as from Fig. 5 is the distinct spatial coherence of the updrafts reducing R. For precipitation with $\rho q_r \gtrsim 2$ g m^{-3}, the data outliers group in several discrete branches corresponding to those model grid columns containing the main updraft. Besides, we see that the largest amounts of precipitation (above 10 g m^{-3}) must have occurred at or below cloud base: for these high values of ρq_r no more R-reduction due to updrafts takes place. Instead, considerable shift towards stronger rain rates indicative of downdrafts exists. While the largest instantaneous rain rate at the ground for this modeled cumulonimbus was 420 mm h^{-1}, the absolute maximum is $R \approx 600$ mm h^{-1}.

4. Discussion

The results of our modeling study showed that the Z–R relations analytically derived for air at rest remain robust in a statistical sense even under strong vertical motions. The scatter relative to the mean relations, however, was found to be large enough to cover the range of variations in Z–R relations $Z = aR^b$ for convective rainclouds as documented in the literature. Even convection in nonsevere storms can account for a jump from $Z \simeq 205R^{1.54}$ to instantaneous relations like $Z = [202 \pm 95]R^{1.54 \pm 0.11}$, encompassing $Z = 300R^{1.5}$ frequently reported for convective clouds. In addition, when different hydrometeor types having individual fall speeds are present, the variability of b increases also.

Concerning the dominant variation of prefactor a, at least the effects of density variations with height can be corrected using a density profile according to the standard atmosphere. Such an average stratification will be absolutely sufficient from a practical point of view. The variation of air density with height is much larger than perturbations between the standard atmosphere and a measured density profile (e.g. from radiosondes). The latter would imply a Z correction of at most a few hundredths of a dB. As a density correction factor we find from $Z = aR^b$ and Eqs. (16a) and (16b):

$$Z_{\mathrm{corr}} = Z\left(\frac{\rho_{00}}{\rho}\right)^{\alpha b}. \tag{32}$$

Obviously, for precipitation aloft the measured radar reflectivity factor Z has to be increased according to Eq. (32) before any standard sea level Z–R relation can be applied to yield a representative rain rate R. For radar echo tops of 10 km ASL, $\alpha \approx 0.45$, $b \approx 1.55$, and $\rho_{10\ \mathrm{km}} \approx 0.41$ kg m^{-3}, we obtain an enhancement factor of 2.18, i.e. roughly a +3.4 dBZ correction, which should not be neglected when deriving a vertical profile of R within a deep raincloud, even if there might be other deficiencies larger than 3 dBZ in real radar data that are not usually being taken care of (e.g. Ulbrich and Lee, 1999; Campos and Zawadzki, 2000).

Probably more important in practical applications is to consider this density correction factor for base-level reflectivity scans at large range. Base-level values of Z (determined, e.g. from 0.5° PPI scans) are routinely used for precipitation estimation. For this elevation angle, the radar beam will be at 1.5 km AGL for 100-km range, and at 3 km AGL in a distance of 150 km to the radar. The density correction for these height levels is about 0.5 and 1.0 dBZ, respectively. For an improved areal precipitation estimate, this should be accounted for. Indirectly it is included, for example, in the Probability Matching Method (Calheiros and Zawadzki, 1987).

Climatological discrepancies between typical values of N_0 at several specific radar sites can lead to different Z–R relations among even nearby radars, as the prefactors $a_{00,N}$, $a_{00,D}$ of the relations depends on N_0 and D_0 directly, as can be seen from Eqs. (14a) and (14b). In addition, the shape parameter γ plays an important role. In this paper, we do not exclusively assume purely exponential ($\gamma = 1$) spectra for the raindrops as done by Marshall and Palmer (1948). Following the evaluation of Ulbrich (1994) who found $\gamma = 1.71 \pm 1.99$, we choose $\gamma = 2$ and apply this value for comparison. Using $N_0 = 8.0 \times 10^6$ m^{-4}, $D_V = 5.0 \times 10^{-4}$ m, $w_0 = 4.1 \times 10^0$ m s^{-1} $\hat{D} = 1.0 \times 10^{-3}$ m, $\beta = 1/2$, and median diameters from Appendix A, we find for the undisturbed prefactors $a_{00,N}$ and $a_{00,D}$ in SI units:

$$a_{00,N} = \begin{cases} 1.0 \times 10^{-10} \text{ for } (\gamma = 1) \\ 1.6 \times 10^{-10} \text{ for } (\gamma = 2) \end{cases}, \tag{33a}$$

$$a_{00,D} = \begin{cases} 2.0 \times 10^{-13} \text{ for } (\gamma = 1, \quad D_0 = 1.4 \times 10^{-4} \text{ m}) \\ 1.7 \times 10^{-13} \text{ for } (\gamma = 2, \quad D_0 = 1.1 \times 10^{-4} \text{ m}) \end{cases}. \tag{33b}$$

For completeness, we give the according Z–R relations in conventional units (Z in mm^6 m^{-3} R in mm h^{-1}) as well:

$$Z = \begin{cases} 305R^{14/9} \text{ for } (\gamma = 1) \\ 464R^{14/9} \text{ for } (\gamma = 2) \end{cases}, \tag{34a}$$

$$Z = \begin{cases} 54.8R \text{ for } (\gamma = 1, \quad D_0 = 1.4 \times 10^{-4} \text{ m}) \\ 46.6R \text{ for } (\gamma = 2, \quad D_0 = 1.1 \times 10^{-4} \text{ m}) \end{cases}. \tag{34b}$$

For weak convection, and in stratiform clouds, at least a portion of the variability in Z–R must be due to variations in the spectra of involved (mixed-phase) hydrometeors. Here two aspects should be considered: cloud physical and orographic peculiarities in

the vicinity of a specific radar site and the occurrence of unusual particle spectra (e.g. Richter and Goddard, 1996; Sauvageot and Koffi, 2000).

One example of the latter would be precipitation-size particle spectra violating the common assumption in many studies of $N_0 = \text{const}$ and rather tending to $D_0 = \text{const}$. In general, precipitation-size particle spectra cannot uniquely be described by assuming constant values of N_0 or D_0. Instead, both are functions of time and space (e.g. Huggel et al., 1996; Nystuen, 1999). However, the case $D_0 \simeq \text{const}$ having been labeled "rare" by Waldvogel (1974) might serve as an explanation for $Z–R$ relations with exponents in the range $[1 \leq b \lesssim 7/5]$ shown in Fig. 1 by light grey shading. In these cases, usually related to precipitation changes from stratiform to convective or vice versa, particle spectra appear to be dominated by $D_0 = \text{const}$, implying $Z \propto R$ and a minor contribution from spectra with $N_0 = \text{const}$. Especially in microphysical equilibrium within shafts of heavy rain, these kinds of spectra can occur in connection to deep convection as well (Zawadzki and de Agostinho Antonio, 1988; Rinehart, 1997). However, due to the overwhelming effect of vertical motions on the $Z–R$ relations, they are likely to be overlooked in the data.

A mesoscale cloud model like KAMM using a bulk microphysical scheme, which specifies spectral shape homogeneously and stationarily for the whole model domain cannot quantify effects like the one just described above. While our analytical investigation retained all degrees of freedom containing hydrometeor spectra, the bulk model results are less general. Focusing on the study of a short-lived summer season rain shower certainly limits the probability of temporal changes in hydrometeor spectra. Nevertheless, the model cloud is likely to be considerably simplified compared to a real rainstorm. Yet, the effect of vertical drafts on R (and hence on $Z–R$) is so dominant in convective clouds that a bulk cloud model with high spatial resolution was adequate to confirm the main findings from the general analytical approach: large deep convection effects on prefactor a, while exponent b is only affected by mixtures or phase changes of hydrometeors.

Comparing our results to those of other investigators, most research on $Z–R$ relations in convective precipitation regions has been carried out from an observational point of view. From her analysis of many observed cases, Austin (1987) was able to show that the actual rain rate in convective downdrafts may double compared to the rain rate derived from the reflectivity factor alone. Also supported by Illingworth and Blackman (1999), this is exactly the finding of the present work. The KAMM modeling results indicated the X-factor from Eq. (19) to reach just the value of $X = 2$. These points are also addressed by Dölling et al. (1998). The authors present a method to quantify the effects of spectral variations. Illingworth and Blackman (1999) estimate the potential error in deriving R from Z up to a factor of two, i.e. 100%.

Atlas et al. (1995) noted the very strong reduction of the measured R in updraft cores. This finding agrees with our value of $X \simeq -0.99$ for the updraft-dominated grid points in the KAMM simulation. In the same article, Atlas and his coauthors experimentally showed the large variations in the prefactors a when $Z–R$ relations were separately derived for up- and downdraft regions. They concluded: "$Z–R$ relations in the presence of significant drafts are meaningless".

This drastic conclusion, although valid for small ensembles taken from strongly different regions inside a cloud or precipitation core, could not be corroborated within our analytical and modeling study. Instead, on average over a whole cumulonimbus

cloud and its precipitation shaft, customary Z–R relations still hold in a statistical sense. This result coincides with yet another experimental study of Z–R relations (Yuter and Houze, 1997). Their main conclusion was that though some far outliers may appear in an R, Z-diagram, on average, the mean relationship between the two remains little affected. Furthermore, they suggested not to distinguish between "stratiform" and "convective" Z–R relations, as these tend to merge and collapse into a single relation. Also, they noted the dependence of experimentally derived reflectivity–rain rate relationships on the spatial scales under consideration. As stated by Atlas et al. (1995) and visible in Figs. 5 and 6 of our present study, considering only a limited volume of a storm to evaluate $R(Z)$ can produce almost any functional form—leading these authors to their drastic statement given above.

Yet, another ambiguity arises from large percentages of hydrometeors like snow or larger cloud ice crystals with $\overline{w}_{t,00} \approx \text{const}$, as these tend to increase the power b of radar-derived Z–R relations. For instance, if the Z–R relationship from Eq. (31) is recomputed, but including reflectivities and sedimentation rates of all hydrometeors, the result from Eq. (31) is changed to

$$Z = [116 \pm 93]R^{1.70\pm0.23}, \quad R = [16.47 \pm 10.26](\rho q_r)^{1.12\pm0.17}. \tag{35}$$

Here inclusion of the large portion of cloud ice in the upper parts of the cumulonimbus cloud alters both prefactor and exponent b. The variation in b brings it close to the value of 2. This ice phase effect due to contributions from different hydrometeor types with substantial reflectivities but highly variable sedimentation rates may also serve as an explanation for empirically found Z–R relations, which display an exponent $b>7/4$, such as the snow relation given by Sekhon and Srivastava (1970) with $b=2.21$:

$$Z = 1780R^{2.21}.$$

While exponents $b>7/4$ are not supported from our evaluation based on well-defined unimodal mean hydrometeor spectra, they could also be evaluated from the data in Fig. 5 if the low rain rate outliers only are considered for $R \gtrsim 0.1$ mm h^{-1}. Such a subset of information easily yields $b \simeq 2.5$ which would, however, lead to a serious contradiction to the physics of the falling hydrometeor ensemble under the assumptions made here (cf. Dotzek, 1999).

The present study has focused on vertical convective motions. However, deep moist convection also has horizontal components and is usually superposed to strong vertically sheared mean horizontal air flow (cf. Houze, 1997). For a developing rain cell with no rain at the ground yet (i.e. $R_{00}=0$), application of a Z–R relation would erroneously diagnose $R_{00} \neq 0$ and also a precipitation accumulation on the ground. In reality, rain will only reach the ground at later times and with a horizontal displacement due to combination of convection and transport by the mean wind profile. While having a minor effect over large areas with homogeneous orography, this horizontal shift can become important over complex terrain with small distances between neighboring river catchments. This is even more so due to the large horizontal gradients of reflectivity in convective clouds (cf. Zawadzki, 1984).

5. Conclusions

This paper has assessed the effects of convective air motion and density stratification on $Z–R$ relations $Z = aR^b$ widely used in radar meteorology. Both analytical and mesoscale model results showed the following:

- Vertical air motions as well as density variations affect the prefactor a of standard $Z–R$ relations, altering both its average value and standard deviation. As a rule of thumb, deep convection primarily increases and density stratification secondarily diminishes the prefactor of average $Z–R$ relations.
- Concerning exponent b of $Z–R$ relations without influence of deep convection, the case $Z \propto R$ represents a lower bound for hydrometeor spectra with scaling diameter $D_0 = \text{const}$ while an upper bound exists with mean terminal velocity $\overline{w}_{t,00} = \text{const}$, leading to $Z \propto R^{7/4}$.
- The only mechanism which could further alter the exponent b of $Z–R$ relations is a change in the terminal fall speed law, which in turn implies variations of hydrometeor *type* or *mixture*. In particular, observed values of the exponent larger $b = 7/4$ are likely to be caused by hydrometeor mixtures.
- In the statistical mean over the whole cloud volume, $Z–R$ relations originally proposed for air at rest and sea level conditions remain applicable even in the presence of deep convection.
- The influence of the vertical density gradient on R can be corrected for using the standard atmosphere density stratification, giving also the opportunity to improve quantitative base-level rainfall estimates at large range (>100 km) from a radar.
- For deep cumulus convection, spatio-temporal variations of instantaneous $Z–R$ relations may be explained by convective drafts. However, although these cover a similar range as variations in statistical $Z–R$ relations for deep convection, the latter are very likely to be affected by other processes also.
- For more stratiform clouds with smaller vertical velocities and cloud depths, prominent differences among empirical $Z–R$ relations likely have to be attributed to variations of the hydrometeor spectra or types in different synoptic situations or different climatological regions.

Proper clarification of how the effects of horizontal convective components and a mean environment wind profile can be included into a radar-derived precipitation accumulation over complex terrain in convective weather situations remains an issue for future research.

Acknowledgements

We are grateful to Martin Löffler-Mang, Ronald Hannesen, and Jürg Joss for many fruitful discussions, and to three anonymous referees for their insightful comments and suggestions.

Appendix A. Median diameters

In contrast to other characteristic diameters of a hydrometeor spectrum, the median diameters with respect to either the total particle number (D_N) or volume (D_V) are probably

the most robust spectral size scales. With N denoting total particle number density, they are defined by

$$\int_0^{D_N} n(D)\mathrm{d}D = \frac{N}{2}, \quad \frac{\pi}{6}\rho_\mathrm{h}\int_0^{D_V} n(D)D^3\mathrm{d}D = \frac{\rho q}{2}. \tag{36}$$

For the Γ-function of Eq. (2), these quantities cannot be analytically evaluated except for very simple cases, e.g. for an exponential size distribution ($\gamma = 1$), the number median is $D_N = \ln 2\, D_0$. In general, D_N and D_V must be numerically evaluated from

$$\sum_{k=0}^{\infty} \frac{(-1)^k}{k!}\frac{D_N(\gamma)^{k+\gamma}}{k+\gamma} = \frac{\Gamma(\gamma)}{2},$$

$$\sum_{k=0}^{\infty} \frac{(-1)^k}{k!}\frac{D_V(\gamma)^{k+\gamma+3}}{k+\gamma+3} = \frac{\Gamma(\gamma+3)}{2}.$$

Obviously, $D_V(\gamma) = D_N(\gamma+3)$. Table 1 shows the two median diameters for several integer values of γ. To a very good approximation, and provided $\gamma \geq 1$, D_V can be written as

$$D_V \simeq (2.67+\gamma)D_0.$$

Using this result and Eq. (9b), Kessler's approach to substitute the $\overline{w}_{\mathrm{t},00}$ relation by the fall speed of a single hydrometeor of diameter D_V is easily verified:

$$\overline{w}_{\mathrm{t},00} = w_0\frac{\Gamma(\gamma+3+\beta)}{\Gamma(\gamma+3)}\left[\frac{D_V}{(2.67+\gamma)\hat{D}}\right]^{\beta}.$$

References

Adrian, G., Fiedler, F., 1991. Simulation of unstationary wind and temperature fields over complex terrain and comparison with observations. Contrib. Atmos. Phys. 64, 27–48.

Aniol, R., Riedl, J., Dieringer, M., 1980. Über kleinräumige und zeitliche Variationen der Niederschlagsintensität. Meteor. Rundsch. 33, 50–56.

Atlas, D., Willis, P., Marks, F., 1995. The effects of convective up- and downdrafts on reflectivity–rain rate relations and water budgets. Proc. 27th Int. Conf. on Radar Meteor., Vail. Amer. Meteor. Soc., Boston, pp. 19–22.

Austin, P.M., 1987. Relation between measured radar reflectivity and surface rainfall. Mon. Weather Rev. 115, 1053–1070.

Battan, L.J., 1973. Radar Observation of the Atmosphere. Univ. Chicago Press, Chicago, 324 pp.

Battan, L.J., 1976. Vertical air motions and the Z–R relation. J. Appl. Meteor. 15, 1120–1121.

Bielli, S., Roux, F., 1999. Initialisation of a cloud-resolving model with airborne Doppler radar observations of an oceanic tropical convective system. Mon. Weather Rev. 127, 1038–1055.

Calheiros, R.V., Zawadzki, I., 1987. Reflectivity–rain rate relationships for radar hydrology in Brazil. J. Clim. Appl. Meteor. 26, 118–132.

Campos, E., Zawadzki, I., 2000. Instrumental uncertainties in Z–R relations. J. Appl. Meteor. 39, 1088–1102.

Clark, T.L., 1974. A study in cloud phase parameterization using the gamma distribution. J. Atmos. Sci. 31, 142–155.

Dölling, I.G., Joss, J., Riedl, J., 1998. Systematic variations of Z–R-relationships from drop size distributions measured in northern Germany during seven years. Atmos. Res. 47–48, 635–649.

Dotzek, N., 1998. Numerische Modellierung topographisch induzierter hochreichender konvektiver Wolken. Ann. Meteor. 37, 465–466.

Dotzek, N., 1999. Mesoskalige numerische Simulation von Wolken- und Niederschlagsprozessen über strukturiertem Gelände. Dissertation, Univ. Karlsruhe, 127 pp. [Available from http://www.op.dlr.de/~pa4p/].

Dou, X., Testud, J., Amayenc, P., Black, R., 1999. The concept of normalized gamma distribution to describe raindrop spectra, and its use to parameterize rain relations. Proc. 29th Int. Conf. on Radar Meteor., Montreal. Amer. Meteor. Soc., Boston, pp. 625–627.

Douglas, R.H., 1964. Hail size distributions. Preprints World Conf. on Radio Meteor. and Proc. 11th Radar Meteor. Conf., Boulder. Amer. Meteor. Soc., Boston, pp. 146–149.

Doviak, R.J., Zrnić, D.S., 1993. Doppler Radar and Weather Observations, 2nd edn. Academic Press, San Diego, 562 pp.

Foote, G.B., du Toit, P.S., 1969. Terminal velocity of raindrops aloft. J. Appl. Meteor. 8, 249–253.

Haddad, Z.S., Durden, S.L., Im, E., 1996. Parameterizing the raindrop size distribution. J. Appl. Meteor. 35, 3–13.

Hauser, D., Roux, F., Amayenc, P., 1988. Comparison of two methods for the retrieval of thermodynamic and microphysical variables from Doppler radar measurements: application to the case of a tropical squall line. J. Atmos. Sci. 45, 1285–1303.

Houze, R.A., 1997. Stratiform precipitation in regions of convection: a meteorological paradox? Bull. Am. Meteor. Soc. 78, 2179–2196.

Huggel, A., Schmid, W., Waldvogel, A., 1996. Raindrop size distributions and the radar bright band. J. Appl. Meteor. 35, 1688–1701.

Illingworth, A.J., Blackman, T.M., 1999. The need to normalise RSDs based on the gamma RSD formulation and implications for interpreting polarimetric radar data. Proc. 29th Int. Conf. on Radar Meteor., Montreal. Amer. Meteor. Soc., Boston, pp. 629–631.

Kessler, E., 1969. On the distribution and continuity of water substance in atmospheric circulation. Meteor. Monogr. 10 (32) Amer. Meteor. Soc, Boston, 84 pp.

Klemp, J.B., Wilhelmson, R.B., 1978. The simulation of three-dimensional convective storm dynamics. J. Atmos. Sci. 35, 1070–1096.

Liu, C.L., Illingworth, A.J., 2000. Toward more accurate retrievals of ice water content from radar measurements of clouds. J. Appl. Meteor. 39, 1130–1146.

Locatelli, J.D., Hobbs, P.V., 1974. Fall speeds and masses of solid precipitation particles. J. Geophys. Res. 79, 2185–2197.

Markowitz, A.H., 1976. Raindrop size distribution expressions. J. Appl. Meteor. 15, 1029–1031.

Marshall, J.S., Palmer, W.M.K., 1948. The distribution of raindrops with size. J. Meteorol. 5, 165–166.

Nystuen, J.A., 1999. Relative performance of automatic rain gauges under different rainfall conditions. J. Atmos. Oceanic Technol. 16, 1025–1043.

Pruppacher, H.R., Klett, J.D., 1997. Microphysics of Clouds and Precipitation, 2nd edn. Kluwer Academic Publishing, Dordrecht, 954 pp.

Richter, C., Goddard, J.W.F., 1996. The dependence of dropsize distribution shape factor on precipitation events. Proc. 12th Int. Conf. on Clouds and Precipitation, Zurich, pp. 61–64.

Rinehart, R.E., 1997. Radar for Meteorologists, 3rd edn. Rinehart Publ., Grand Forks, 428 pp.

Sauvageot, H., 1992. Radar Meteorology. Artech House, Boston, 366 pp.

Sauvageot, H., Koffi, M., 2000. Multimodal raindrop size distributions. J. Atmos. Sci. 57, 2480–2492.

Sekhon, R.S., Srivastava, R.C., 1970. Snow size spectra and radar reflectivity. J. Atmos. Sci. 27, 299–307.

Sekhon, R.S., Srivastava, R.C., 1971. Doppler observations of drop size distributions in a thunderstorm. J. Atmos. Sci. 28, 983–994.

Sempere Torres, D., Porrà, J.M., Creutin, J.-D., 1994. A general formulation for raindrop size distribution. J. Appl. Meteor. 33, 1494–1502.

Sempere Torres, D., Porrà, J.M., Creutin, J.-D., 1998. Experimental evidence of a general description for raindrop size distribution properties. J. Geophys. Res. 103D, 1785–1797.

Smith, P.L., 1984. Equivalent radar reflectivity factors for snow and ice particles. J. Clim. Appl. Meteor. 23, 1258–1260.

Smith, P.L., Myers, C.G., Orville, H.D., 1975. Radar reflectivity factor calculations in numerical cloud models using bulk parameterizations of precipitation. J. Appl. Meteor. 14, 1156–1165.

Soong, S.-T., Ogura, Y., 1973. A comparison between axisymmetric and slab-symmetric cumulus cloud models. J. Atmos. Sci. 30, 879–893.

Starr, D.O'C., Cox, S.K., 1985. Cirrus clouds: Part I: A cirrus cloud model. J. Atmos. Sci. 42, 2663–2681.

Tartaglione, N., Buzzi, A., Fantini, M., 1996. Supercell simulations with simple ice parameterization. Meteor. Atmos. Phys. 58, 139–149.

Ulbrich, C.W., 1983. Natural variations in the analytical form of the raindrop size distribution. J. Clim. Appl. Meteor. 22, 1764–1775.

Ulbrich, C.W., 1994. Corrections to empirical relations derived from rainfall disdrometer data for effects due to drop size distribution truncation. Atmos. Res. 34, 207–215.

Ulbrich, C.W., Lee, L.G., 1999. Rainfall measurement error by WSR-88D radars due to variations in $Z–R$ law parameters and the radar constant. J. Atmos. Oceanic Technol. 16, 1017–1024.

Waldvogel, A., 1974. The N_0-jump of raindrop spectra. J. Atmos. Sci. 31, 1067–1078.

Willis, P.T., 1984. Functional fits to some observed drop size distributions and parameterization of rain. J. Atmos. Sci. 41, 1648–1661.

Yuter, S.E., Houze, R.A., 1997. Measurements of raindrop size distributions over the Pacific warm pool and implications for $Z–R$ relations. J. Appl. Meteor. 38, 847–867.

Zawadzki, I., 1984. Factors affecting the precision of radar measurements of rain. Proc. 22th Int. Conf. on Radar Meteor., Zurich. Amer. Meteor. Soc., Boston, pp. 251–256.

Zawadzki, I., de Agostinho Antonio, M., 1988. Equilibrium raindrop size distributions in tropical rain. J. Atmos. Sci. 45, 3452–3459.